Ice Boom Simulations and Experiments

Mark A. Hopkins[1] and Andrew M. Tuthill[2]

Abstract: A three-dimensional discrete element model (DEM) was developed to simulate ice boom operation in a rectangular channel. The model simulates the motion of each individual ice floe, the interaction between adjacent floes, the interaction of the floes with the walls and boom, and the water drag applied to the floes on the underside of the ice accumulation. The DEM simulations were compared with a parallel set of physical model tests using natural ice. The DEM successfully reproduced the observed magnitude and distribution of the forces on the boom and the channel sides as the boom retained a surge of drifting ice. Variations in channel side roughness produced similar changes in the division of forces between the boom and sidewalls in the simulations and model tests. Finally, the load distribution between the boom and the channel sides and the effect of channel side roughness in the context of granular ice-jam theory were analyzed.

CE Database keywords: Three-dimensional models; Ice jams; Simulation; Channels, waterways.

Introduction

Ice booms, the most widely used type of ice control structure, have advantages of relatively low cost and minimal environmental impact. Over the past half-century, ice boom design methods have evolved from simple water velocity and Froude number criteria (Perham 1983) to the use of unsteady, two-dimensional numerical ice-hydraulic models (Shen et al. 1997). Important issues addressed in ice boom design are the stability of the ice cover upstream of the boom and the ice load on the boom. From experiments in a small power canal, Latyshenkov (1946) observed that as ice accumulates behind a boom the increase in force on a boom

[1]U.S. Army Cold Regions Research and Engineering Laboratory, 72 Lyme Rd., Hanover, NH 03755.

[2]U.S. Army Cold Regions Research and Engineering Laboratory, 72 Lyme Rd., Hanover, NH 03755.

Note. Discussion open until February 1, 2003. Separate discussions must be submitted for individual papers. To extend the closing date by one month, a written request must be filed with the ASCE Managing Editor. The manuscript for this paper was submitted for review and possible publication on April 17, 2001; approved on March 21, 2002. This paper is part of the ***Journal of Cold Regions Engineering***, Vol. 16, No. 3, September 1, 2002. ©ASCE, ISSN 0887-381X/2002/3-138–155/$8.00+$.50 per page.

levels off once the ice cover progresses to a length of approximately 2.5–3 channel widths. Perham and Racicot (1975) found that in subfreezing air temperatures, the boom force may level off in as little as 1.5 river widths. Advances in the theory of river ice cover formation further aided boom designers. Pariset and Hausser (1966) found a critical upstream water velocity for stable ice cover formation, and Ashton (1974) and Daly and Axelson (1990) defined hydraulic conditions for the under turning of floes at the upstream edge of an ice cover.

Physical model testing and experimental field projects have also advanced the state of the art in ice boom design. Innovative projects include the boom on the South Platte at Casper, Wyoming (Burgi 1971), the Allegheny River ice boom (Deck and Gooch 1984), and the Salmon River ice boom (White 1992). In addition, during the past decade, the Canadian Coast Guard has developed effective, durable, low-cost booms constructed of steel pipe through field testing on the lower St. Lawrence River (Morse, personal communication) and physical model tests at Fleet Technology Ltd., Kanata, Ontario, Canada.

Shen et al. (1997) developed an unsteady 2D ice-dynamic model that accurately simulated ice retention and ice transport over the multispan Lake Erie-Niagara River ice boom. Discrete Lagrangian parcels represented the ice field by incorporating ice characteristics such as floe thickness, concentration, and the internal strength of ice accumulation into the model ice rheology. The ice loading on an individual boom span was assumed to be uniform, and ice overtopped the boom when a critical cable tension was exceeded. Liu and Shen (2000) refined the ice stoppage criteria, added a capability for calculating the horizontal load distribution along the boom spans, and used the model to simulate ice retention at proposed sites on the lower Missouri River.

In this work, a newly developed 3D discrete-element model (DEM) (Hopkins et al. 1996) was used to simulate the use of a segmented cylindrical ice boom to retain a floating layer of circular ice floes in a rectangular channel. The floes are driven by water drag applied to the underside of the ice cover. The forces exerted by the ice on the ice boom and on the channel walls are calculated at each time step. The results of the computer simulations are compared with results from similar physical model experiments performed in the refrigerated research area of the ice engineering facility at the U.S. Army Cold Regions Research and Engineering Laboratory (CRREL). The channel dimensions and important material parameters used in the simulation were measured from the model experiments. The direct comparison between simulations and model experiments covered three discharges and two wall roughness conditions.

Mechanics of Simulation

A discrete element model is a computer program that explicitly models the dynamics of a system of discrete particles. In these simulations, the particles are the individual ice floes and boom segments. The position, orientation, velocity, and shape of each floe and boom segment are stored in arrays. At each time step, the contact and body forces on each floe and segment are calculated, and they are moved to new locations with new velocities that depend on the resultant of the

forces. A detailed description of the mechanics of the simulation used in this work is given by Hopkins et al. (1996). The following summary of important details is taken from Hopkins and Tuhkuri (1999).

The ice floes in the simulations are flat disks with a circular edge. The floes are formed by dilating a flat disk of radius R_1. In the dilation process in mathematical morphology (Serra 1986), the 2D circular disk is transformed into a 3D disk with a thickness of $h=2R_2$ and a diameter of $d=2(R_1+R_2)$ by placing the center of a sphere with a radius of R_2 at every point on the 2D circular disk. The aspect ratio of the floe d/h can be varied by changing R_1 and R_2. The top and bottom surfaces of the floes are flat.

Contact detection, the crux of any discrete element code, is handled by an iterative method. The 2D circular disk of radius R_1 at the core of each floe is called a constraint surface. The external surface of the floe is, at all points, a distance of R_2 from the constraint surface. When two disks are found to be in proximity (by standard grid methods), a vector is arbitrarily placed with its head on the constraint surface of one floe and its tail on the constraint surface of the other floe. This vector is modeled as an elastic band whose ends are connected to frictionless sliders that are constrained to remain on the two constraint surfaces. Pulled by its elasticity, the head and tail of the vector move iteratively to locations on the constraint surfaces that define the shortest distance between the two floes. If the length of the vector is less than $2R_2$, then the floes are in contact. The vector, which is perpendicular to the external surfaces of the two floes, defines the normal to the contact surface.

Wherever two floes touch the overlap is interpreted as a deformation of the floes resulting in a contact force. The contact force has components normal and tangential to the surfaces at the point of contact. The normal axis $\vec{n}$ is perpendicular to the surface of each floe. The tangential axis $\vec{t}$ is in the direction of the tangential component of the relative velocity at the point of contact. The normal component of the contact force F_n is

$$F_n=k_n\delta-\eta\vec{V}_{1/2}\cdot\vec{n} \tag{1}$$

where k_n=normal contact stiffness; η=normal contact viscosity; and $V_{1/2}$=relative velocity of floe 1 with respect to floe 2 at the point of contact. A value of η near critical damping is used to produce highly inelastic behavior. Tensile forces are not modeled. The incremental change in the frictional tangential force is proportional to the relative tangential velocity. The tangential force F_t is

$$\vec{F}_t^n=\vec{F}_t^{n-1}-k_t\Delta t\vec{V}_{1/2t} \tag{2}$$

where the superscript n denotes the current time step; Δt=time step; and k_t =tangential contact stiffness that is set to 60% of k_n. The relative tangential velocity $\vec{V}_{1/2t}$ is defined as

$$\vec{V}_{1/2t}=\vec{V}_{1/2}-\vec{V}_{1/2}\cdot\vec{n} \tag{3}$$

If the tangential force F_t exceeds the Coulomb limit μF_n where μ=friction coefficient, then the contact begins to slip, and the x, y, and z components of F_t

are scaled such that $|F_t| = \mu F_n$. The magnitude of k_t affects the rate at which the frictional force increases to the Coulomb limit μF_n. The moments on each floe are calculated from the forces and moment arms.

Water drag was calculated using a quadratic drag law. The channel was divided into 1-m-long sections. The drag calculation in the streamwise (x) direction in each section was calculated from the difference between the average water velocity and the average ice velocity in the section. The equation for the water drag in the x-direction in a section with length x is

$$D_x = \frac{1}{2}(w\Delta x) C_d \rho_w (V_w - V_x)|V_w - V_x| \tag{4}$$

where $w\Delta x$ ($\Delta x = 1$ m) = planar area of the section and ρ_w = water density. The average ice velocity in the x-direction V_x was calculated by averaging the velocities of all floes whose centers lay in the section between adjacent crosssections. The average water velocity V_w and drag coefficient C_d were measured in the model experiments and were assumed to be constant over the entire channel. The water drag D_x on the section was divided evenly among the individual floes whose centers lay in the section and were visible from a point on the channel bed directly beneath the floe. Floes whose centers were not visible from the channel bed were either located in the interior of or on top of other floes. Water drag in the y- and z-directions was based on individual floe velocities. The equation for drag F_{dy} on a floe in the y-direction where the average water velocity was zero was

$$F_{dy} = \frac{1}{2} A C_d \rho_w V_y |V_y| \tag{5}$$

where $A = (R_1^2 + R_2^2)$ is the floe area and $V_y = y$-component of the floe velocity. The drag in the z-direction and the rotational drag were calculated similarly and applied to the individual floes. The buoyant force and its moment on each floe were calculated using look-up tables based on the depth of the center of the floe and the inclination of the floe normal with respect to the water surface. The tables were generated from computer integration of the submerged volume of the circular disk-shaped floes prior to the simulation. Water surface slope and porous flow were neglected in the simulations. It was estimated that the streamwise component of the weight of the ice contributed at most approximately 8% of the total streamwise load on the frame, and the streamwise force from the porous flow was less.

After the program calculates the sum of the forces and torques exerted on each floe, the equations of motion for each floe are solved, and time is advanced. The translational equations of motion use simple central difference approximations. Changes in the angular velocities and orientation of the floes are much more complicated to calculate. A method developed by Walton and Braun (1993) was used. Euler's equations of motion for the time derivatives of the angular velocities in the principal body frame are solved using a predictor-corrector algorithm. Floe orientations are specified by four parameters called quaternions (Evans and Murad 1977). The updated quaternions are found by solving central-difference approximations for the time derivatives of the quaternions, expressed in terms of the quaternions themselves and the angular velocities.

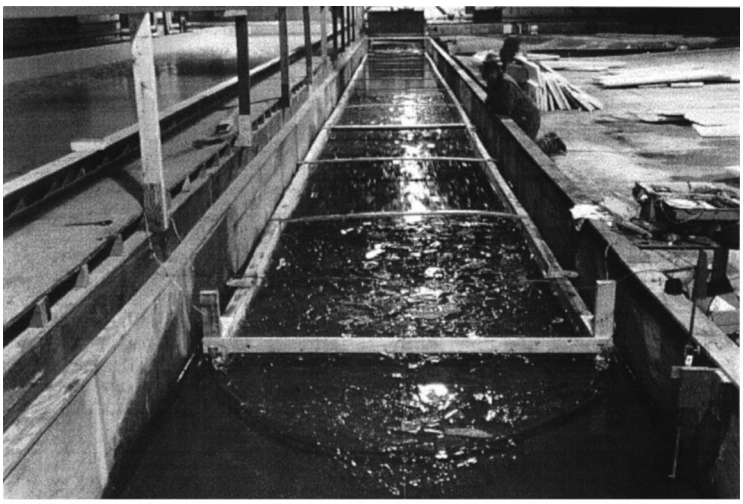

Fig. 1. Experiment looking up the channel. The ice boom is in the foreground. The crosspieces in the picture connect the sides of a frame suspended from load cells at the far end of the channel. The ice cover is in motion in the region upstream of the second crosspiece.

In each simulation, the change in the kinetic and potential energy of the floes and the energy dissipated by inelastic and frictional contacts and water drag are calculated at each time step. Inelastic and frictional dissipation are determined by computing the work performed by the normal and tangential components of each contact force. The energy balance is used to gauge numerical accuracy. In the simulations described below, the error in the energy balance was less than 2%.

Model Experiments: Ice Retention using Ice Boom in Rectangular Channel

The model experiments were performed in a 2.25×36-m-long refrigerated flume, shown in Fig. 1, located in the ice engineering facility at CRREL. The flume had a rectangular cross-section. A 1.95×25 m floating, rectangular wooden frame (shown in Fig. 1) was placed in the flume. The frame was suspended in the stream by two 0–110 N load cells that were attached to the upstream end of the frame and anchored to the flume walls. Two types of wall coverings were used in the experiments: smooth walls of bare polystyrene attached to the inside of the frame and rough walls created by covering the polystyrene with expanded plastic mesh composed of 44-mm-wide by 3-mm-deep diamond-shaped elements. The model ice boom consisted of seven 28×305 mm wooden cylinders tethered to a span cable, as shown in Fig. 2. The ends of the cable were attached through 0–44 N

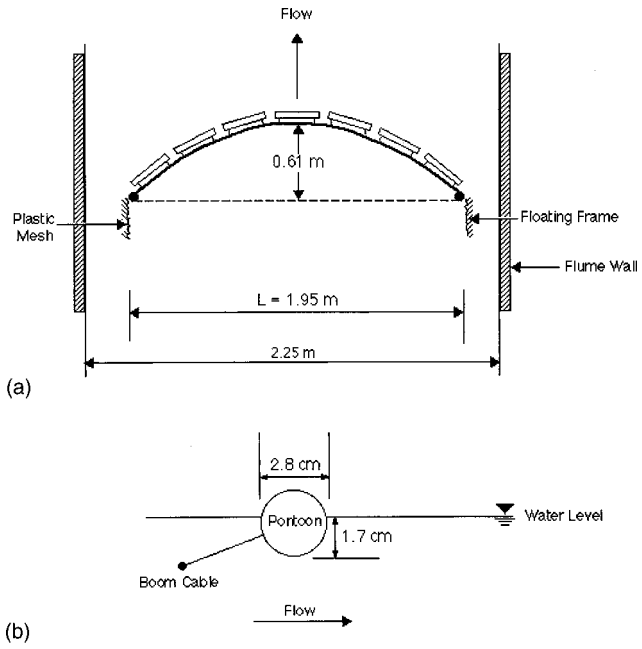

Fig. 2. Diagram of boom used in physical model experiments: (a) Plan view of ice boom; (b) Cross section of ice boom

load cells to the downstream end of the frame. This arrangement allowed measurement of both the total streamwise load on the frame and the downstream force acting on the boom.

A uniform sheet of freshwater ice was grown in the feed tank located to the left of the flume in Fig. 1. The doors to the room were opened, and the room was allowed to warm-up. The average air and water temperatures were 1.7 and 0.4°C, respectively. Each ice sheet was broken into angular pieces or floes with an average diameter of 135 mm and an average thickness of 15 mm. Table 1 lists characteristics of the piece size distributions for the model ice in model dimen-

Table 1. Ice Floe Average Thickness and Size Distribution

Ice type	$\langle h \rangle$ (m)	D_{15} (m)	D_{50} (m)	D_{85} (m)	Porosity
Model ice	0.015	0.075	0.135	0.185	0.45[a]
(prototype at 1:25 scale)	0.38	1.9	3.4	4.6	
Missouri River ice	0.25	1	3	7	0.4–0.5[b]

[a]Calculated from measured ice and water mass and volume.

[b]Estimated.

Table 2. Model Discharge, Depth, and Velocity

Model channel discharge (m^3/s)	Model depth (m)	Model average open water velocity (m/s)	Prototype open water velocity (m/s)	Froude number
0.043	0.173	0.127	0.635	0.097
0.053	0.182	0.151	0.755	0.11
0.058	0.185	0.163	0.815	0.12

sions, at the 1:25 prototype scale, and for floe sizes measured from aerial photographs of drifting ice on the lower Missouri River.

The floes were carried downstream from the feed basin into the flume. A temporary barrier, placed across the flume 6.7 m upstream of the boom, held the arriving ice until the upstream extent of the ice cover reached a point 24 m upstream of the boom. With the ice cover at rest, the cover thickness was measured at 1.22 m intervals. The temporary barrier was then removed, allowing the ice to drift downstream until it reached the boom.

Test series were conducted at the steady discharges listed in Table 2. The intention was to represent, at 1:25 scale, the range of water depth and velocity conditions found on the lower Missouri River during heavy ice periods. Conventional ice boom design theory gives an upper limit velocity of about 0.7 m/s and a maximum Froude number of about 0.1 for successful ice retention behind a boom (Perham 1983). The hydraulic conditions modeled in this study were chosen to bracket these criteria. A sharp-crested weir controlled flow depth at the downstream end of the flume. Each discharge was tested using rough and smooth wall conditions, and three to five tests were made with each combination of discharge and wall roughness.

Comparison with Ice Boom Model Experiments

A parallel set of simulations were performed, similar to the model experiments, with the computer model described above. The main differences between the simulations and the experiments were in the geometry of the ice floes and the hydraulic conditions. The floes in the experiments were polygonal ice pieces broken from a sheet with a distribution of sizes and a fairly uniform thickness. The simulated floes were cylindrical disks with uniform diameters and thicknesses that were approximately the same as the experimental floes. The hydraulic conditions existing in the experiments were reproduced in a simple fashion by using average water velocities and drag coefficients. The drag coefficient for each experiment was calculated from the average under-ice shear stress obtained by dividing the total load on the frame by the area of the ice cover. Two values of the drag coefficient and water velocity in each simulation were used. The first values were calculated with the ice cover at equilibrium behind the temporary barrier. The second values were calculated when the ice cover reached equilibrium behind the segmented ice boom. The increased ice accumulation thickness in this

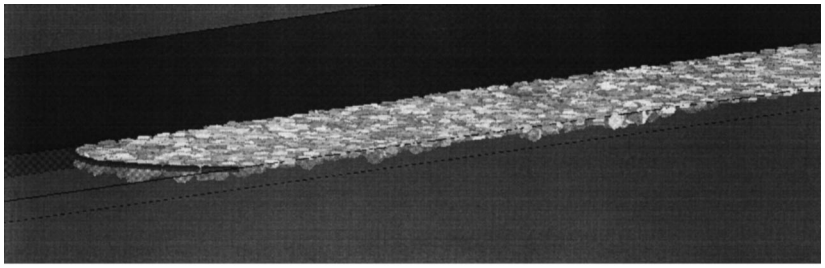

Fig. 3. Scene from a simulation. The segmented ice boom is at left. The near bank has been removed to reveal the ice cover made up of disk-shaped floes.

phase increased both the drag coefficient and the water velocity. The simulated boom was composed of seven cylindrical segments with the same length, diameter, and density as the model boom. The sag of the boom was also the same.

The simulations were performed in the same way as the experiments. A temporary barrier was placed in the channel 6.7 m upstream of the boom. The floes entered the flume, floated down the channel, and collected at the temporary barrier until a cover was created that was the same length as the preliminary ice cover in the experiments. The first values of the drag coefficient Cd_1 and water velocity Vw_1 were used in this phase of the simulation. After the cover was formed, the temporary barrier was removed. With the barrier removed, the floes moved downstream until they reached the ice boom. The second values of the drag coefficient Cd_2 and water velocity Vw_2 were used in this phase of the simulation. The simulation continued until all of the floes stopped. A scene from a simulation is shown in Fig. 3. The segmented boom is shown on the left in Fig. 3, while the near wall is cut away to reveal the cover.

We used a friction coefficient μ_s of 0.35 in the simulations for contacts involving the flat surfaces of the floes. A larger friction coefficient μ_e of 0.9 was used for contacts involving the circular edges of the floes to approximate the effect of the vertical edges of the floes used in the physical experiments that impeded rafting. Although the friction coefficients μ_s and μ_e are quite high by usual standards, we felt that they might compensate to some degree for the incipient freezing observed in the model experiments. We used a friction coefficient μ_b of 0.9 for contacts between the floes and the boom and a friction coefficient μ_w for contacts with the channel walls that had a value of 1.0 in rough-wall simulations and 0.1 in smooth-wall simulations. In addition, in rough-wall simulations we placed vertical cylinders along the walls on both sides of the channel to create a no-slip condition similar to the effect created by the corners of the floes interacting with the coarse mesh in the experiments. The cylinders had the same diameter as the floes and extended from the bed to a short distance above the water surface. The cylinder centers were spaced 1.5 diameters apart. The parameters used in the simulations are listed in Table 3.

In a discrete element simulation, the contact stiffness k_n, used to calculate the normal contact force Eq. (1), must be sufficient to make the overlaps between the

Table 3. Parameters used in Simulations

Parameter	Value
L, channel length	36.6 m
w, channel width	1.95 m
h, floe thickness	15 mm
d, floe diameter	140 mm
ρ_i, ice density	920 $kg \cdot m^{-3}$
ρ_w, water density	1000 $kg \cdot m^{-3}$
k_n, normal contact stiffness	2000 $N \cdot m^{-1}$
η, normal contact viscosity	5.15 $kg \cdot s^{-1}$
μ_s, ice/ice flat surface friction	0.35
μ_e, ice/ice edge friction	0.9
μ_b, ice/boom friction	0.9
μ_w, ice/wall friction	0.1, 1.0
t, time step	0.001 s

neighboring floes negligible. The maximum contact forces in the present simulations were approximately 0.25 N, corresponding to a maximum overlap of about 0.1 mm (less than 1% of the floe thickness) using the value of k_n shown above. The number of floes varied between 1,800 and 4,500, depending on the water drag during the initial build-up period. The approximate run time for a 250 s simulation with 4,000 floes was 4 h on a 800 MHz Pentium 3 computer.

We compared the simulation results with the experimental results at the three flow rates shown in Table 2 for both the smooth- and rough-wall conditions discussed above. The results obtained in the model experiments and simulations are summarized in Table 4. The results are averages of three to five experiments and simulations.

The average layer thickness H in the experiments was measured at 1.22 m intervals by pushing an L-shaped probe having a 120 mm foot through the ice cover and raising it until it first touched the underside of the ice. We calculated the average layer thickness in the simulations by simulating the lowering of a 30-mm diameter probe from above and raising of a probe from beneath the layer of floes until the probes contacted the upper and lower surfaces of the layer. This was repeated at 1,000 random locations in the floe field. The results of the simulation for the rough-wall case at the highest flow rate are missing because the boom was unable to stop the ice. The boom in the experiments was also near its limit at the highest flow rate. It failed to stop the ice in two of six cases. Neither the simulation nor the experimental boom was able to stop the ice at the highest flow rate in a channel with smooth walls.

To simulate ice boom performance, it is necessary to closely match the under-ice drag, the roughness of the channel walls, and the rubble strength of the layer of rafted and underturned floes. Under-ice drag was matched by the expedient of using the average water velocities and calculated drag coefficients from the experiments. The roughness of the channel walls determines the division of the total

Table 4. Comparison of Results between Experiments and Simulations

Discharge (m^3/s)	Wall surface	Type	Cd_1	Cd_2	Vw_1 (m/s)	Vw_2 (m/s)	F_{boom} (N)	F_{wall} (N)	H_1 (mm)	H_2 (mm)	Length (m)
0.043	Rough	Experiment	0.039	0.053	0.141	0.153	2.6	9.2	17	30	9.9
		Simulation	0.039	0.053	0.141	0.153	3.8	10.8	15	19	12.4
0.053	Rough	Experiment	0.035	0.077	0.172	0.215	7.8	27.6	26	60	10.4
		Simulation	0.035	0.077	0.172	0.215	10.9	23.2	31	54	10.0
0.058	Rough	Experiment	0.046	0.074	0.209	0.267	10.5	42.3	43	78	10.4
		Simulation	—	—	—	—	—	—	—	—	—
0.043	Smooth	Experiment	0.027	0.041	0.139	0.154	7.5	3.0	18	35	10.9
		Simulation	0.027	0.041	0.139	0.154	7.9	3.1	20	32	12.0
0.053	Smooth	Experiment	0.033	0.055	0.190	0.207	18.7	7.8	39	51	11.5
		Simulation	0.033	0.055	0.190	0.207	20.1	6.4	45	73	11.2

Note: Cd_1, Vw_1, and H_1 are the drag coefficient, water velocity, and average layer thickness during the initial build-up.

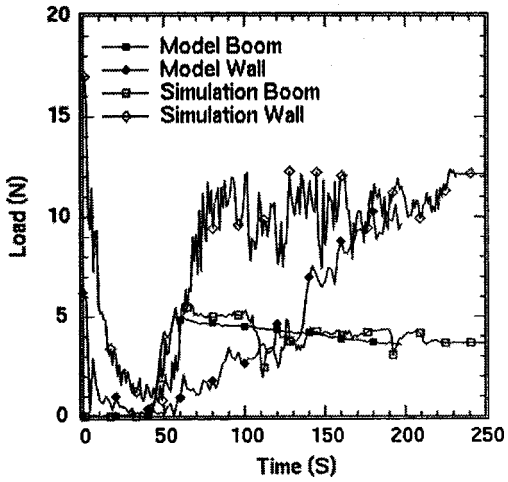

Fig. 4. Comparison of boom and wall forces measured in the experiments with forces calculated in the simulations. The walls were rough, and the discharge was 0.043 m^3/s.

load between the boom and walls. As Table 4 shows, in rough-wall cases, the walls carry more force than the boom, while in smooth-wall cases the opposite occurs. In the experiments, the vertices of the angular ice floes penetrated the mesh on the channel sides to create a no-slip condition. The boundary conditions in the simulation were adjusted to obtain a similar division between the boom force and wall force. The two features of the wall conditions that were adjusted to mimic the experimental wall conditions were the friction coefficient used in floe-wall contacts and the placement of vertical cylinders along the walls. The cylinders were spaced 1.5 diameters apart. By transmitting tangential force to the walls through normal, nonfrictional contact forces, the cylinders behave like the expanded mesh attached to the walls in the experiments, creating a no-slip boundary condition.

The rubble strength of the ice floes is a function of their shape and friction coefficient. In addition, in the experiments, the rubble strength also depends on the amount of freezing between floes, which was small but appreciable. The diameter and thickness of the floes in the simulations were approximately the same as the average diameter and thickness of the floes in the experiments. The ice-on-ice friction coefficient μ_s used in the simulations was probably somewhat high for freshwater ice, but may compensate for the incipient freezing observed in the experiments. In addition, a separate friction coefficient μ_e was used in edge contacts to make rafting between simulated floes with circular edges better simulate rafting between model floes with square edges. The reasonably good agreement between the average rubble layer thickness in the simulations and experiments in Table 4 indicates that the rubble strengths are matched fairly well.

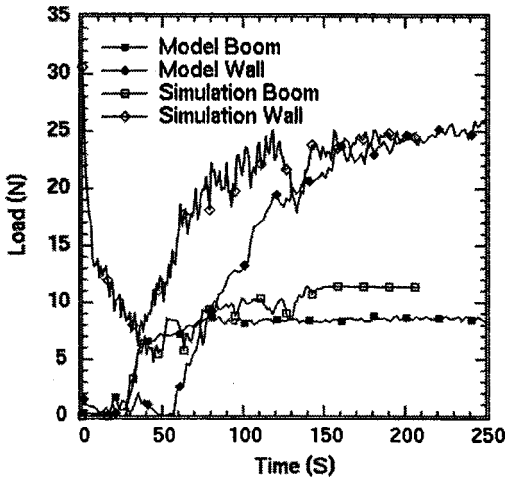

Fig. 5. Comparison of boom and wall forces measured in the experiments with forces calculated in the simulations. The walls were rough, and the discharge was 0.053 m^3/s.

Comparison with Ice Jam Theory

The forces on the boom and sidewalls in the rough-wall simulations and experiments are shown in Figs. 4 and 5. The forces in the smooth-wall simulations and experiments are shown in Figs. 6 and 7. In the rough-wall simulations and experiments, the wall forces are larger than the boom forces, while in the smooth-wall cases, the reverse is true. The obvious explanation for this is that the smooth walls cannot carry as much load as the rough walls. Because the boom must carry what the walls cannot, the wall roughness controls the partition of the drag force between the walls and the boom. In ice-jam theory (Pariset et al. 1966) the under-ice shear force is balanced by the longitudinal force f, with dimensions of Nm^{-1}, in the ice cover and the shear force on the channel edges. The force balance on a control volume spanning a channel of width B can be expressed as

$$Bdf + 2\mu_1 f dx = \tau B dx \tag{6}$$

The first term in Eq. (6), Bdf, is the difference between the longitudinal force on the upstream and downstream faces of the control volume. The second term, $2\mu_1 f dx$, is the shear or tangential force on the sides of the control volume. The coefficient μ_1 is the product of the active pressure coefficient K_1 that relates the longitudinal force to the transverse force and the effective friction coefficient μ that relates the transverse force to the tangential force on the channel edge. The third term is the water drag force on the underside of the control volume that is the product of the shear stress τ and the area. The solution of Eq. (6) is

$$f^* = \frac{1}{2\mu_1}(1 - e^{-2\mu_1 x^*}) \tag{7}$$

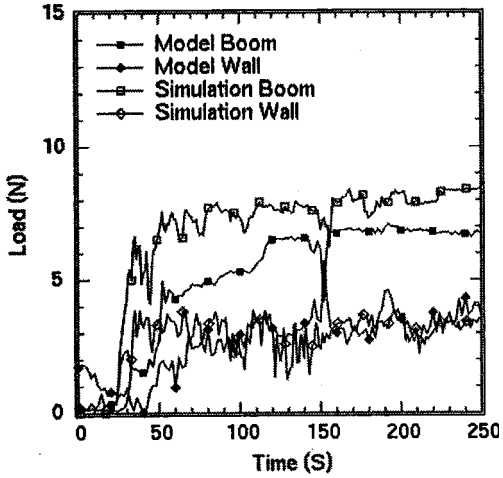

Fig. 6. Comparison of boom and wall forces measured in the experiments with forces calculated in the simulations. The walls were smooth, and the discharge was 0.043 m^3/s.

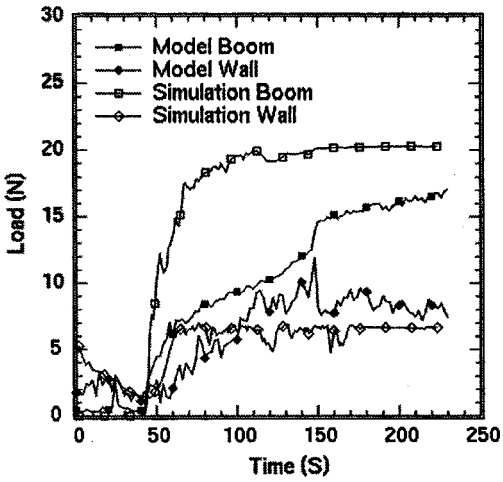

Fig. 7. Comparison of boom and wall forces measured in the experiments with forces calculated in the simulations. The walls were smooth, and the discharge was 0.053 m^3/s.

Table 5. Ice-Jam Theory Parameters Derived from Simulation Results

Discharge (m^3/s)	Wall surface	$f_n/f\ (K_1)$	$f_t/f_n\ (\mu)$	$f_t/f\ (\mu_1)$	f^*_{max}	x^*_{max}
0.043	Rough	0.854	0.367	0.375	1.33	3.07
0.053	Rough	0.574	0.591	0.349	1.43	3.30
0.043	Smooth	0.686	0.096	0.067	7.46	17.2
0.053	Smooth	0.573	0.082	0.052	9.62	22.1

where f and x are nondimensionalized as

$$f^* = f/\tau B \quad \text{and} \quad x^* = x/B \tag{8}$$

For large x^*, the limiting value of f^* is $1/2\mu_1$. At the end of each simulation, with the ice cover in equilibrium, the longitudinal force f, transverse force f_n, and shear force f_t, were calculated in control volumes two floe diameters in length beginning at the upstream end of the jam. The shear force f_t was the x-direction component of the force between the floes and the channel walls. In the case of the bumpy boundaries in the rough-wall simulations, this was not limited to the force component that is tangential to the bumpy surface at a point of contact. The results averaged over the entire length of the jam for each simulation are given in Table 5.

The first parameter, the active pressure coefficient K_1, is a function of the floe properties such as friction coefficients, density, and aspect ratio that were the same in all four simulations. The second parameter, μ, depends on wall roughness. In the smooth-wall simulations, μ is determined by the friction coefficient μ_w. However, μ is less than μ_w because not all of the contacts are fully mobilized, that is, not slipping or about to slip. In the rough-wall simulations, μ is a complicated function of μ_w and the bumpy boundaries. Table 5 shows that the effective friction coefficient μ is clearly different for the two boundary conditions. In the smooth-wall case, μ is slightly less than μ_w. The third parameter, μ_1, the product of K_1 and μ in each section, is fairly consistent for each boundary condition. The fourth column shows the limiting force obtained by substituting the values of μ_1 in Table 5 into Eq. (7). The fifth column shows the distance from the upstream end of the jam x^*_{max} where f^* reaches 90% of the limiting value given in column 4, obtained by solving Eq. (7) for x^*. The two rough-wall cases reach this level in slightly more than three channel widths, while the smooth-wall cases require much longer extents. The variation in the longitudinal force f^* as a function of channel position for the four cases is shown in Fig. 8. Because the longitudinal force f^* is noisy, we plot the surrogate difference between the under-ice shear force and the wall shear beginning at the upstream end of the ice cover in each simulation. The plot of the difference is smooth because the under-ice shear and the wall shear are integrated quantities. The boom is located at $x^* = 13.7$ in Fig. 8.

The two rough-wall plots of f^* in Fig. 8 reach a maximum that is close to the predicted value shown in Table 5. They reach those maximum values at a distance of about three channel widths from the upstream end, as predicted in Table 5. The smooth wall plots of f^* in Fig. 8 fall far short of the predicted maximum values

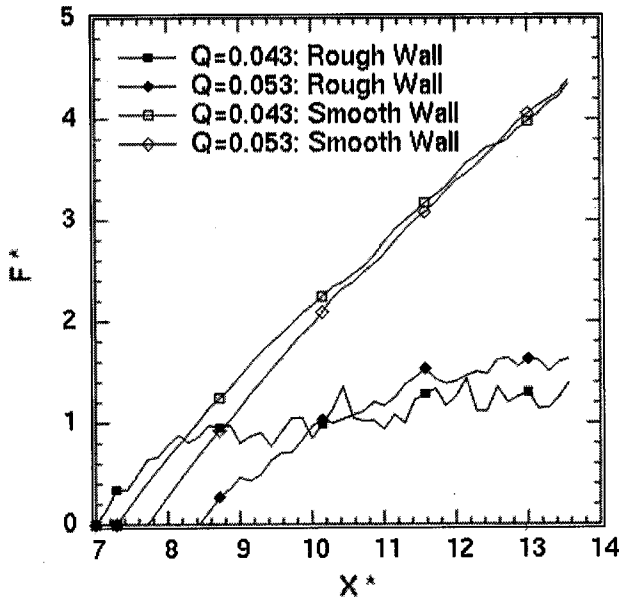

Fig. 8. Integrated sum of the wall shear and the under-ice shear forces as a function of channel position for the two discharges and degrees of wall roughness. The forces were calculated after each simulation had reached equilibrium. The ice boom is located at $X^* \approx 13.8$. The force and position are nondimensional.

in Table 5. The accumulation lengths in the smooth-wall simulations of about seven channel widths are much shorter than the 17–22 channel widths that, according to theory, are necessary for the longitudinal force in the ice cover to reach its maximum. The maximum force in Fig. 8 is both the part of the under-ice shear force not balanced by the wall shear, as well as the force the ice exerts on the boom. It is interesting to observe that the deficit is passed from the upper end of the ice cover, through the equilibrium region (if any) to the boom. It is also interesting to observe that, for a given river width, ice volume, and discharge, it is the roughness of the channel sides that determines the force on the boom.

The longitudinal force f^* that is transmitted through the ice cover is zero at the upstream end of the jam and increases in the downstream direction until the equilibrium section of the jam (if any) is reached and then remains roughly constant until the boom is reached, as shown in Fig. 8. According to ice-jam theory, where the longitudinal force is increasing the accumulation should thicken to carry the additional load. The longitudinal force f and the accumulation thickness H are related by the equation (Uzuner and Kennedy 1976)

$$f = \frac{1}{2}(1-n)\rho_i g(1-\rho_i/\rho_w)\left(\frac{1+K_1}{1-K_1}\right)H^2 \tag{9}$$

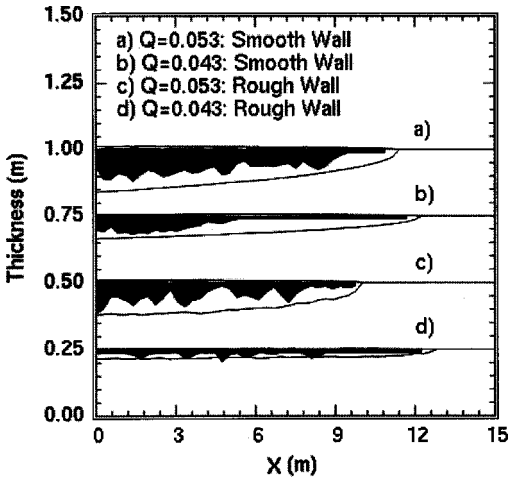

Fig. 9. Ice cover thickness versus channel position calculated in the simulations. The boom is located at zero. The solid lines enveloping the profiles are the profiles calculated from ice-jam theory.

where n=porosity of the ice accumulation. Fig. 9 shows the variation in the thickness of the ice accumulation as a function of channel position for the same four simulations. Thickness was calculated at 1,000 points in the channel. The point values in each meter-long segment were averaged. The simulation thickness profiles are shown as black-filled saw-tooth-shaped areas. The envelopes surrounding the simulation thickness profiles were obtained by inverting Eq. (9) to obtain H and using the dimensional values of the forces from Fig. 8 along with the parameters from Tables 3 and 5. A porosity n of 50% was assumed. Experimental thickness results are not presented because the measurements, spaced 1.22 m apart along the channel centerline, were too sparse to capture the thickness variation with any accuracy.

Conclusions

A 3D discrete element computer model was developed to simulate the use of a segmented ice boom to retain drifting ice in a river. The results of simulations performed with the computer model were compared with results of a parallel series of physical model experiments performed in the refrigerated research facility of ice engineering at CRREL. Parallel DEM simulations and physical model tests at two flow rates and with two channel wall roughness conditions produced force versus time graphs that are qualitatively and quantitatively similar. The DEM model has the capability to be a valuable design and analysis tool because of its ability to simulate the 3D dynamics of individual ice pieces as well as the interaction of ice pieces with the boom and channel walls or river banks.

In addition to verifying the DEM, we also compared the results of the simulations to ice-jam theory (Pariset et al. 1966; Uzuner and Kennedy 1976). This was done by calculating the longitudinal force in the ice cover, the transverse force on the channel walls, and the tangential force on the channel walls at the end of each simulation with the ice cover at rest. Using the calculated average values of the active pressure coefficient and the effective wall friction coefficient, the maximum longitudinal force and equilibrium jam length predicted by ice-jam theory were close to the simulations results.

The under-ice shear in the simulations was not calculated from hydraulic conditions. Instead, we used average values of the drag coefficient and water velocity measured in the experiments. This removed the burden of having to correctly simulate hydraulic conditions and facilitated our comparison with ice-jam theory in which drag is also an input. Although we used average experimental values for the drag coefficient and water velocity in the simulations, this is not equivalent to setting the force levels on the boom and walls. The total force on the boom and the walls at equilibrium as well as the partition of the total load between the boom and the walls depend on the under-ice shear, the area of the ice cover, the roughness of the channel walls, and the rubble strength of the layer of rafted and underturned floes. The accuracy of the simulation is determined by how well the roughness of the channel walls and the rubble strength of the floes are modeled. The roughness of the channel walls was adjusted by varying the friction coefficient and by attaching roughness elements to the walls. The rubble strength of the floes was adjusted by varying the friction coefficient and the aspect ratio of the floes.

Acknowledgments

This work was funded under work unit No. 33132: ''Numerical Modeling of Ice Processes'' of the CRREL Cold Regions Engineering Research Program and by a CRREL in-house laboratory independent research grant. Steven Daly gave us advice and insight about the problem. Gordon Gooch of CRREL was instrumental in the physical model construction and testing.

References

Ashton, G. D. (1974). ''Froude criterion for ice block stability.'' *J. Glaciol.*, 13(68), 309–313.

Burgi, P. H. (1971). ''Ice control structure on the North Platte River: A hydraulic model study.'' *REC-ERC-71-465*, U.S. Department of the Interior, Bureau of Reclamation, Washington D.C.

Daly, S. F., and Axelson, K. D. (1990). ''Stability of floating and submerged blocks.'' *IAHR J. Hydraul. Res.*, 28(6), 737–752.

Deck, D. and Gooch, G. (1984). ''Performance of the Allegheny River ice control structure, 1983.'' *Special Rep. 84-13*, U.S. Army Cold Regions Research and Engineering Laboratory, Hanover, N.H.

Evans, D. J., and Murad, S. (1977). ''Singularity free algorithm for molecular dynamics simulation of rigid polyatomics.'' *Mol. Phys.*, 34(2), 321–326.

Hopkins, M. A., and Tuhkuri, J. (1999). ''Compression of floating ice fields.'' *J. Geophys. Res.*, 104(C7), 15815–15825.
Hopkins, M. A., Daly, S. F., and Lever, J. H. (1996). ''Three-dimensional simulation of river ice jams.'' *Proc., 8th Int. Specialty Conf. on Cold Regions Engineering, ASCE*.
Latyshenkov, A. M. (1946). ''A study of protective ice booms.'' *Gidrotechnicheskiye Stroitel'stvo*, 15(4), 13, in Russian.
Liu, L., and Shen, H. T. (2000). ''Numerical simulation of river ice control with booms.'' *ERDC/CRREL Tech. Rep.*, Army Cold Regions Research and Engineering Laboratory, Hanover, N.H.
Pariset, E., Hausser, R., and Gagnon, A. (1966). ''Formation of ice covers and ice jams in rivers.'' *J. Hydraul. Div.*, 92(6), 1–24.
Perham, R. E. (1983). ''Ice sheet retention structures.'' *CRREL Rep. 83-30*, U.S. Army Cold Regions Research and Engineering Laboratory, Hanover, N.H.
Perham, R. E., and Racicot, L. (1975). ''Forces generated on and ice boom on the Beauharnois Canal.'' *Proc., 3rd Int. Symp. on Ice Problems*, U.S. Army Cold Regions Research and Engineering Laboratory, Hanover, N.H., 397–407.
Serra, J. (1986). ''Introduction to mathematical morphology.'' *Comput. Vis. Graph. Image Process.*, 35, 283–305.
Shen, H. T., Lu, S., and Crissman, R. D. (1997). ''Numerical simulation of ice transport over the Lake Erie-Niagara River ice boom.'' *Cold Regions Sci. Technol.*, 26, 17–33.
Uzuner, M. S., and Kennedy, J. F. (1976). ''Theoretical model of river ice jams.'' *J. Hydraul. Div.*, 102(9), 1365–1383.
Walton, O. R., and Braun, R. L. (1993). ''Simulation of rotary-drum and repose tests for frictional spheres and rigid sphere clusters.'' *Joint DOE/NSF Workshop on Flow of Particulates and Fluids*, Cornell Univ., Ithaca, N.Y.
White, K. D. (1992). ''Salmon River experimental ice boom, 1989–90 and 1990–91 winter seasons.'' *Special Rep. 92-20*, U.S. Army Cold Regions Research and Engineering Laboratory, Hanover, N.H.